Towards practical solid-state lithium-sulfur batteries: challenges and perspectives

Saneyuki Ohno[a*], Wolfgang G. Zeier[b,c*]

[a]*Department of Applied Chemistry, Graduate School of Engineering, Kyushu University, 744 Motooka, Nishi-ku, 819-0395 Fukuoka, Japan*

[b]*Institute of Inorganic and Analytical Chemistry, University of Münster, Corrensstrasse 28, 48149 Münster, Germany*

[c]*Helmholtz Institut Münster, Forschungszentrum Jülich, Corrensstrasse 46, D-48149 Münster, Germany.*

Emails:

saneyuki.ohno@cstf.kyushu-u.ac.jp

wzeier@uni-muenster.de

CONSPECTUS:

The energy density of the ubiquitous lithium-ion batteries is rapidly approaching its theoretical limit. To go beyond, a promising strategy is the replacement of conventional intercalation-type materials with conversion-type materials possessing substantially higher capacities. Among the conversion-type cathode materials, sulfur constitutes a cost-effective and earth-abundant element with a high theoretical capacity that has a potential to be game-changing, especially within an emerging solid-state battery configuration. Employment of non-flammable solid electrolytes that improves battery safety and boosts the energy density, as lithium metal anodes are also viable. The long-standing inherent problem of conventional lithium-sulfur batteries, arising from the reaction intermediates dissolved in liquid electrolytes, can be eliminated with inorganic solid ion conductors. In particular, the highly conducting and easily processible lithium-thiophosphates have successfully enabled the lab-scale solid-state lithium-sulfur cells to achieve close-to-theoretical capacities. For applications requiring safe, energy-dense, lightweight batteries, solid-state lithium-sulfur batteries are an ideal choice that could surpass conventional lithium-ion batteries.

Nevertheless, there are challenges specific to practical solid-state lithium-sulfur batteries, beyond the typical challenges inherent to solid-state batteries in general. While the conversion reaction of sulfur realizes a large specific capacity, the associated significant total volume changes of the active material results in contact losses among the cathode components and, consequently, decreases reversible capacity. Additionally, the ionically and electronically insulating active material requires composite formation with solid electrolytes and electron-conductive additives to secure sufficient ion and electron supply at a triple phase boundary. However, the compositing process itself makes the carrier transport pathways very tortuous and requires the balancing of carrier transport and optimization of the attainable energy density. Lastly, the requirement of a high interfacial area to establish sufficient triple-phase boundaries promotes the degradation of the solid electrolytes, and the formation of less-conductive interphases further deteriorates the transport in the composites.

This Account focuses on the challenges associated with developing practical solid-state lithium-sulfur

batteries and provides an overview over recently developed concepts to tackle these critical challenges: (1) Introduction of the *conversion efficiency* to enable quantitative assessments of the impact of chemo-mechanical failure. (2) For long-term cycling, the electrolyte degradation at the interface and the electrochemical activity of the formed interphases come into play. Practical stability tests with increased interfacial areas and subsequently altered reversal potentials can quantify the magnitude of the electrolyte degradation and confirm influences of reversible redox activity of the interphases. (3) Monitoring the effective conductivity in the composites clarifies correlations between transport and cyclability, further highlighting the need of quantitative measurements to address the composite carrier transport. (4) Impedance spectroscopy combined with transmission-line model analysis as a function of applied potentials can visualize the *stability window of good effective ion-transport* to utilize both the capacity contributions from redox-active interphases and the high ionic conductivity. In the end, a roadmap toward the practical solid-state lithium-sulfur batteries will be presented.

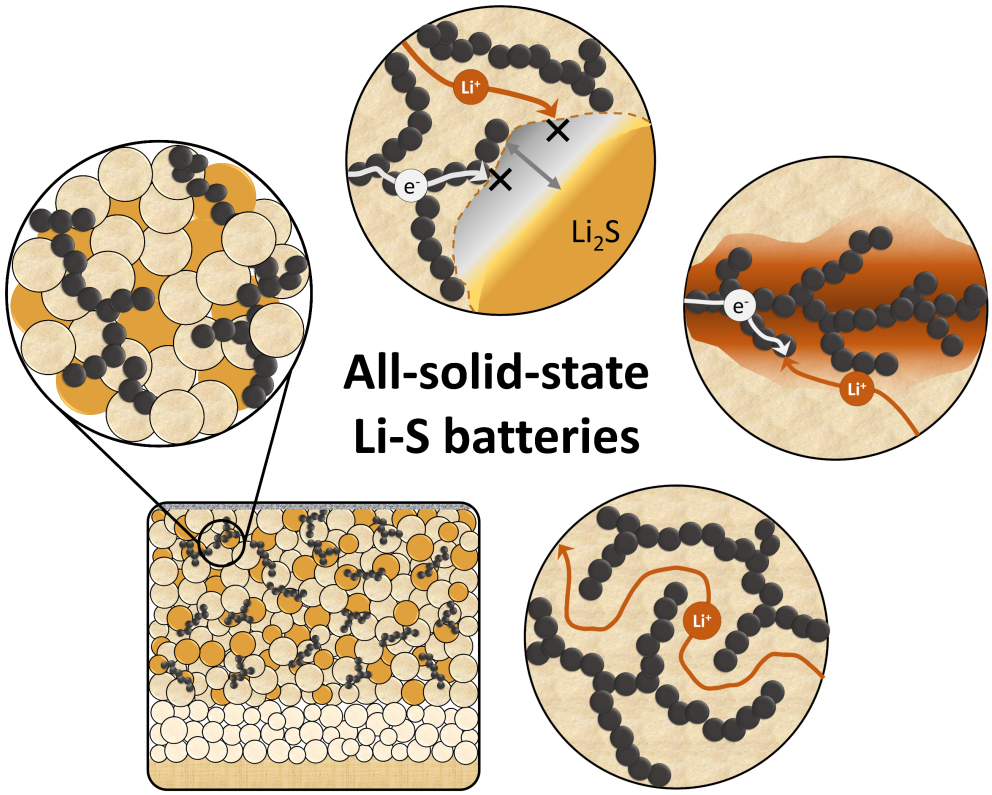

1. Introduction

Lithium-sulfur (Li-S) batteries are a promising candidate for a lightweight, earth-abundant, and cost-effective next-generation energy storage device. Owing to a substantially high specific capacity of sulfur (1672 mAh g_S^{-1}), the energy density of Li-S batteries, especially gravimetric (Wh kg^{-1}), can go far beyond that the conventional Li-ion batteries.[1,2] Ever since Herbert and Ulam patented the first concept of Li-S batteries in the early 1960s,[3] countless efforts have been devoted to developing rechargeable Li-S batteries. However, developmental challenges exist. So far, the critical bottleneck has been the degradation caused by the dissolution of cathode reaction intermediates into the liquid electrolyte. Negatively charged polysulfides can travel from the cathode side to the anode side through the electrolyte (called "shuttle effect") and precipitate on the anode surface, causing a loss of active materials and an increase in the cell resistance.[4] Although the shuttle effect has been reduced by trapping sulfur in the vicinity of the cathode through nanostructuring carbon scaffold, and by introducing a separator that filters polysulfides or even more concentrated electrolyte solutions,[5] implementing all-solid-state battery architecture is a promising alternative strategy. Replacing liquid electrolytes to inorganic solid electrolytes physically prohibits the reaction intermediates from shuttling and is expected to improve battery safety. Together with utilizing the lithium metal anode, a boost in energy density occurs that will pave the way for commercial applications.[6]

Naturally, the essential component enabling a solid-state battery technology is a solid electrolyte. Oxide- and sulfide-based inorganic ion conductors are the two heavily investigated classes of materials. While the oxides possess superior chemical and electrochemical stability, sulfide-based electrolytes typically outperform oxides in ion transport, owing to a more polarizable anionic framework.[7] In addition, the mechanically soft sulfides allow room-temperature pressing to secure dense and intimate contacts between the components.[8] For a more comprehensive overview of various solid electrolytes and their challenges, we refer the reader to recent reviews.[9–12] Towards a Li-S battery application, the usage of easily processible sulfide-based electrolytes becomes imperative. The ionically and electronically

insulating nature of sulfur, and its discharged product Li_2S, requires compositing the sulfur with solid electrolytes and electron-conducting additives to establish a triple-phase boundary, where both the ions and electrons can be provided.

Despite the promising theoretical advantages, there are still various remaining challenges toward practical solid-state Li-S batteries. First, challenges for solid-state batteries remain at a lithium metal anode, and these are reviewed elsewhere.[13,14] The most significant challenges at the solid-state sulfur cathode are illustrated in Figure 1. A large volume expansion and contraction of sulfur upon lithiation and delithiation can cause contact losses in the composite. The so-called chemo-mechanical failure can hinder reversible redox of active materials as contact losses lead to an insufficient transfer of ions and electrons and an effective reduction of triple-phase boundaries (Figure 1a). While a high interfacial contact area among components is vital to fully utilize insulating active materials, a substantial interfacial area between solid electrolytes and electron conductive additives can result in non-negligible electrolyte degradation.[15] This electrolyte degradation leads to the formation of degradation products at the interface, referred to as interphases. The interphases are typically less conductive and deteriorate the cell cycling performance (Figure 1b). Sluggish ion transport in the composite is another critical challenge to solve. An increase in active material loading leads to more tortuous carrier transport pathways, which increases overpotential and may hinder battery performance (Figure 1c). A significant fraction of conducting phases secures sufficient ion and electron transport within the composite; however, the more non-active material there is the less achievable a high energy density becomes. Therefore, improving transport is essential to enhance energy density and cyclability, and underscores the need for quantitative measurements of the transport in the composite. Moreover, each challenge shown in Figure 1 can coincide and influence each other. An already sluggish ion transport can be further worsened by electrolyte degradation, formation of interphases, or cracks and contract losses. In this Account, we provide an overview to these challenges and suggest perspectives toward practical solid-state Li-S batteries.

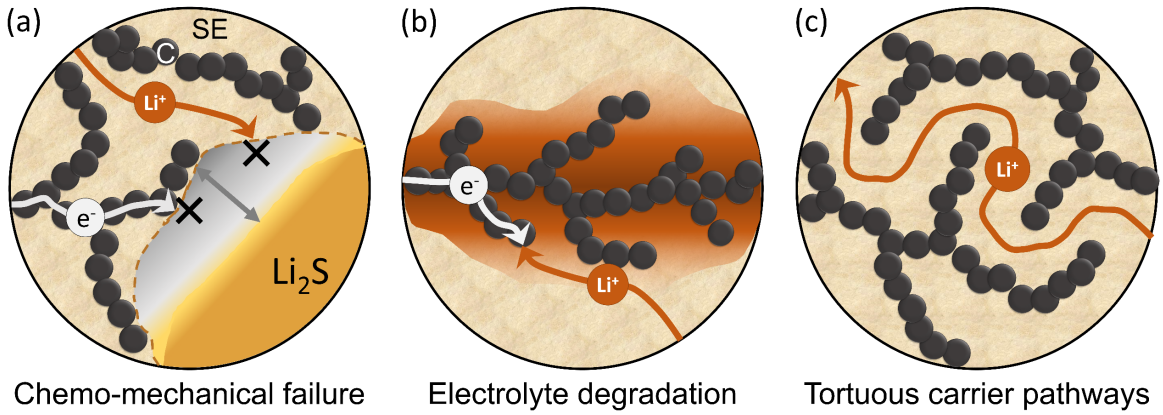

Figure 1: *Significant challenges to solve for solid-state Li-S batteries. (a) Chemo-mechanical failure: volume changes of active material induce contact loss among cathode components, where SE and C are solid electrolytes and carbon. (b) Electrolyte degradation: degradation of sulfide-based electrolytes results in interphases. (c) Tortuous carrier pathways: winding conduction pathways impede fast ion/electron transport in composites.*

2. Challenges

2.1. Chemo-mechanical failure

Volume changes associated with lithiation and delithiation of active materials can cause the formation of cracks and contact losses, deteriorating the cell cycling performance. This "chemo-mechanical failure" is a common challenge for developing solid-state batteries,[16] and is further intensified when materials that undergo larger volume changes are used. Whereas the exact reaction pathway is still open to argument, Li-S battery chemistry relies on the following electrochemical reaction,

$$S_8 + 16\ Li^+ + 16\ e^- \leftrightarrow 8\ Li_2S. \qquad \text{Eq. 1}$$

The volume increase of S_8 with a mole of lithiation amounts to 6.09 $cm^3\ mol^{-1}$ and a full lithiation of one mole of S_8 expands its volume by 79 % by forming 8 moles of Li_2S. The expanded volume will contract by the same amount upon the following delithiation, causing the chemo-mechanical failure influencing both short- and long-term cycling.[17]

When preparing two cathode composites through hand-grinding or ball-milling, with the same amount of sulfur, carbon and solid electrolyte (Li_6PS_5Cl), significant differences in the performance can be

observed, as shown in Figure 2a. Mechanically milling the composite delivers a larger overall capacity as better mixing leads to more triple-phase boundaries, and the following charging shows almost the same capacity as the initial discharge capacity. Conversely, in the hand-ground composite less than 50% of the initial discharge capacity is recharged. X-ray photoelectron spectroscopy (XPS) shows the reason for the underlying loss mechanism (Figure 2b). Ideally, the sulfur peaks (orange doublet, $S_{(0)}$) should disappear and a doublet of Li_2S (green doublet, S^{2-}) should appear upon a discharge. A reverse reaction should occur upon charging for a well-running cell, as seen in the ball-milled cathode. However, in the hand-ground composite, a significant fraction of Li_2S remains unconverted upon the first charging. This irreversible formation of Li_2S after the initial discharge causes a 54 % loss of capacity and can be traced to the initial sulfur particle size. Mechanical milling reduces the sulfur particle size, ultimately mitigating strong detrimental volume effects. Although this initial loss is often overlooked, similar capacity losses in the literature indicate how common this failure mechanism is.[18] Well-processed cathode composites with intimate contacts among the cathode components are needed to suppress the chemo-mechanical loss, highlighting the importance of cathode processing procedures. Naturally, a question of how significantly the chemo-mechanical failure impacts long-term cycling remains.[19] To tackle the question, cycling efficiencies are usable as indicators of how much Li_2S is remained unconverted due to the chemo-mechanical failure.

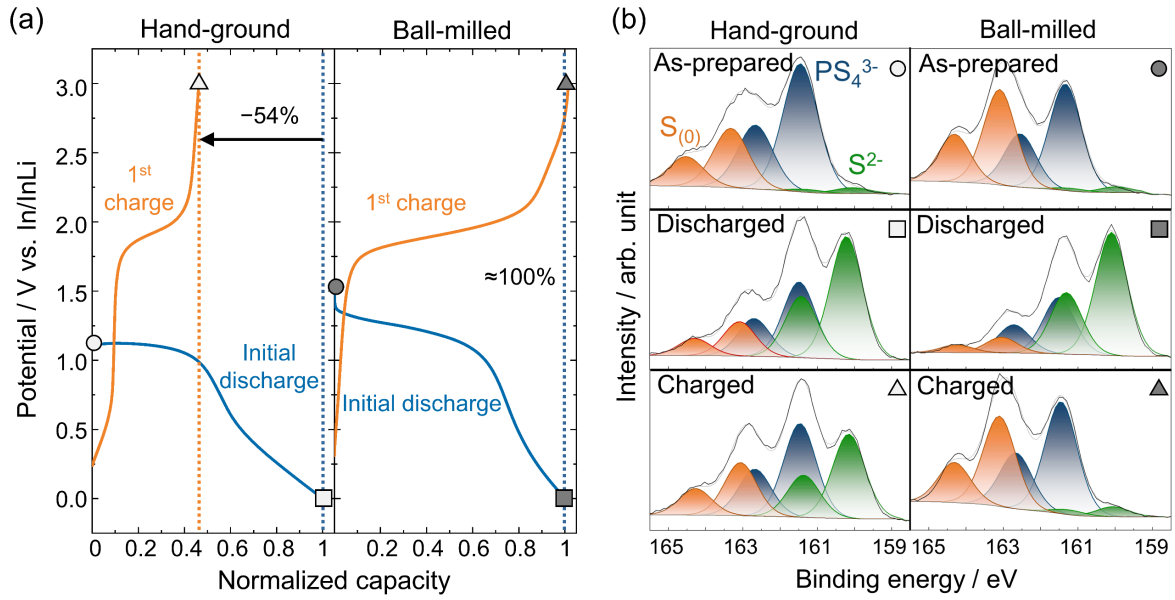

Figure 2: *Impact of chemo-mechanical failure in Li-S batteries:*[17] *(a) Initial discharge and the following 1st charge with hand-ground and ball-milled cathode composites normalized to the initial discharge capacity. (b) S 2p spectra taken by post-mortem XPS on the hand-ground and ball-milled composite cathodes, before electrochemical treatment (As-prepared ○), after the initial discharge (Discharged □), and after the first charge (Charged △). Filled symbols are for the ball-milled composite. The significant capacity loss in the hand-ground composite is due to the irreversible formation of Li_2S. An InLi alloy is employed as the anode to fix the anode potential to In/InLi (0 V vs. In/InLi is 0.62 V vs. Li^+/Li).*

For a quantitative discussion, the definition of cycle efficiencies needs to be revisited: Cell cycling performance is generally presented as the delivered capacity and its corresponding Coulombic efficiency Φ_Q, representing the ratio of charge released during the discharge to the charge necessary for charging the battery in the nth cycle,[20]

$$\Phi_Q \equiv Q_{d,n}/Q_{c,n} \qquad \text{Eq. 2}$$

where $Q_{d,n}$ and $Q_{c,n}$ are the discharged and charged capacity, respectively. This is illustrated in Figure 3a. While the operation of Li-S cells with sulfur as the active materials starts with a discharge, a "cycle" is defined to consist of a charging followed by a discharging, which in turn defines the capacity delivered

before the first charging as an initial discharge capacity. The Coulombic efficiency is useful to assess a fraction of usable charged capacity in the following discharging. However, the amount of recoverable capacity upon charging concerning previous discharging is equally valuable for secondary batteries. Therefore, it is helpful introduce a *conversion efficiency* Φ_C, with

$$\Phi_C \equiv Q_{c,n}/Q_{d,n-1}. \quad \text{Eq. 3}$$

In other words, the Coulombic efficiency describes how much S is converted to Li_2S during a discharge, whereas the conversion efficiency describes how much Li_2S is converted back to sulfur upon charging. Using this definition, the ball-milled cathode exhibits a conversion efficiency of almost 100 %. In contrast, the conversion efficiency of the hand-ground composite shown in Figure 2a is about 46 %, indicating that 54 % of capacity is lost by the irreversible formation of Li_2S.

In order to extend the discussion to long-term cycling and irreversible losses during cycling, Figure 3b shows the observed capacity and Φ_C of a ball-milled cathode over 50 cycles. While Φ_Q is almost 100 %, meaning that the reaction from S to Li_2S is complete, the Φ_C is lower and responsible for the low-capacity retention.[17] Post-mortem analyses on the charged cathode after long-term cycling between 0 – 3 V vs In/InLi revealed that the capacity loss is, again, due to the irreversibly formed Li_2S.[17] Increasing the lower cutoff potential leads to improvements of Φ_C and, with it, enhanced capacity retention. The shallow discharge leads to a lower amount of irreversible formation of Li_2S, as less intense volume changes upon cycling occur, as illustrated in Figure 3c. However, whereas a reduction of the electro-chemomechanical volume changes is needed, an incomplete usage of active material through shallow discharge reduces the achievable capacity. An alternative strategy is needed to mitigate the detrimental influence of volume expansions in solid-state Li-S batteries.

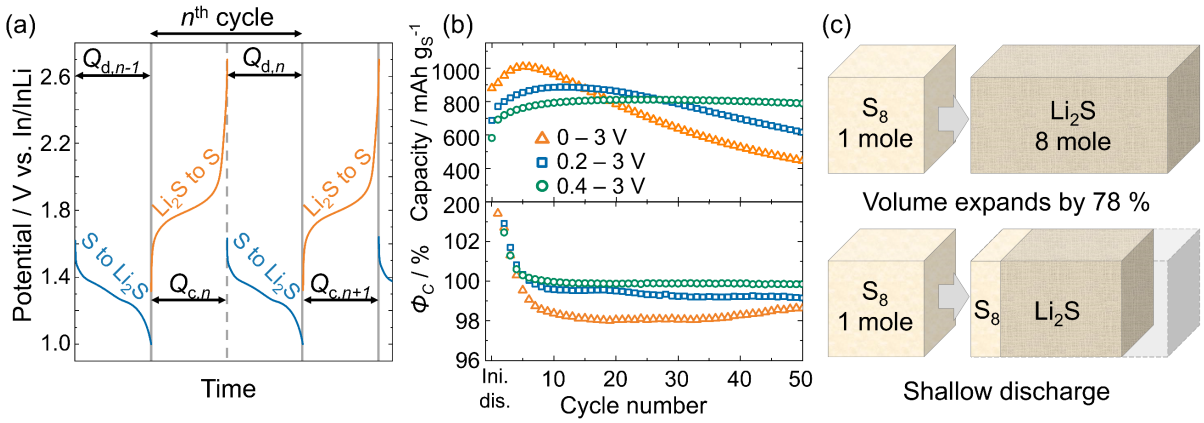

Figure 3: *(a) Exemplary potential profiles of solid-state Li-S batteries at the n-th cycle. (b) Shallow discharge improves long-term capacity retention mainly with enhanced conversion efficiency.*[17] *(c) Sacrificing the total capacity with shallow discharge may help to mitigate the chemo-mechanical failure by reducing the detrimental volume changes.*

2.2. Electrolyte degradation

Whereas volume changes can be detrimental for long-term cycling, additional electrolyte degradation also plays a critical role, especially once the electrolytes are composited with electron conductive additives.[21] Although solid electrolytes are often considered stable, sulfide-based solid electrolytes can degrade at the composite interfaces and form interphases.[15,22] These degradation products are, in contrast to liquid electrolytes, always sticking to the vicinity of the active materials and electron-conducting phases, which ultimately impacts cyclability and transport in the composite itself.[23] This is problematic as solid-state Li-S batteries require a high interfacial area among the components, all of which demand practical assessments of the stability of the employed electrolytes and the influence of interphases upon decomposition.

An approach to measure the electrochemical stability of materials is conventional cyclic voltammetry (CV) tests, in which the electrolytes are sandwiched between planar electrodes such as stainless-steel rods. However, the planar electrode setup exhibits minute reaction current in solids as shown in Figure 4a (blue curve). By using this setup, a sulfide solid electrolyte is seemingly stable within a wide range of electrode potentials. In stark contrast, a thermodynamic calculation indicates minimal stability

windows of Li-thiophosphates, e.g., 1.71 – 2.14 V and 1.71 – 2.01 V vs. Li/Li^+ for $Li_{10}GeP_2S_{12}$ and Li_6PS_5Cl, respectively.[24] The discrepancy between experiment and theory can be attributed to the restricted volume of the electrolyte that can undergo electrochemical degradation as illustrated in Figure 4b.[25,26] By compositing with carbon (C), the interfacial area between electrolytes and electrodes is increased and results in significantly more electrochemical activity (orange curve in Figure 4a). Positive and negative current peaks appear, indicating the occurrence of electrochemical reactions. However, it is unclear if the appearing peaks (e.g., ★ and ☆ in Figure 4a) arise from the oxidation and reduction of electrolytes, or represent a redox activity of the decomposition products.

To further assess the nature of interphases, *stepwise cyclic voltammetry* is helpful with subsequently increasing/decreasing the higher/lower reversal potential after each cycle. This approach can provide information on the redox activity and its reversibility at different potentials. For instance, a stepwise CV with a Li_6PS_5Cl-C composite (Figure 4c) reveals that the peaks at ★ and ☆ are due to reversible redox activity of degradation products, not the electrolyte itself. The early cycles (green to light green curves) suggest kinetic electrolyte stability until a growing reaction current due to SE oxidation can be seen. The distinct peak at around 2.0 V vs. In/InLi (★) only becomes prominent after intense oxidation at a potential of around 2.3 V vs. In/InLi. Once the peaks (★ and ☆) appear, their magnitude increases with further SE oxidation (orange to red curves). The oxidative degradation of Li-thiophosphates leads to amorphous phases with complex P-$[S]_n$-P-type polyanions, e.g. (P_2S_n), Li_2S_n, $Li_3PS_4(\mu\text{-}S_n)S_4PLi_3$ ($(Li_3PS_4)_2S_n$), and -$[S]_n$- containing polysulfides.[15,25–30] The more comprehensive descriptions on oxidative and reductive electrolyte degradation are summarized in references 25 and 26. In short, a kinetic electrochemical stability window for these electrolytes exists, and once the solid electrolytes are decomposed, their decomposition products become redox-active. Ideally, CV measurements require a three-electrode configuration as the CV of the working electrode depend on the counter electrode within a two-electrode configuration unless the potential of the counter electrode is fixed.

The cyclability of these redox-active interphases can then be tested by galvanostatically cycling the solid electrolyte – carbon (SE-C) composite cathode with various cutoff potentials, as shown in Figure 4d.[26]

It should be noted again that the reversible redox activity is caused by the degradation products and not by the solid electrolyte itself. Therefore, we will use the term “apparent capacity” or “apparent redox activity” hereafter to highlight the fact that observed capacity and redox activity are not from the solid electrolyte itself. Cycling between 1 – 1.8 V vs. In/InLi delivers only minimal capacity, indicating that no significant electrolyte degradation occurs. By increasing the upper-cutoff potentials to 2.4 V, 2.7 V, and 3.0 V vs. In/InLi, apparent capacities were delivered, corroborating the formation of redox-active degradation products. The observed capacity increases with increasing upper-cutoff potential, suggesting a more pronounced formation of interphases. Meanwhile, with a deep discharge down to 0 V vs. In/InLi, although a substantially high apparent capacity can be observed, it is irreversible and rapidly fades (Figure 4d). The formation of partially electron-conducting interphases, e.g. Li_3P and LiP (or more generally Li_xP) likely cause progressive degradation at the interface.[26]

Overall, all Li-thiophosphates seem to exhibit similar electrochemical behavior as their sulfur and phosphorous composition generally govern the oxidative and reductive stability.[28,29,31–33] While the reductive electrolyte degradation occurs at relatively low potentials, the potential range causing oxidative electrolyte degradation largely overlaps with the voltage window of a solid-state Li-S battery operation making interphase formation is unavoidable. The reversible redox activity of interphases may help boost the attainable capacity, but the degradation also influences the overall transport within the composite and the cell cyclability. These influences will be discussed in the following section.[26,34]

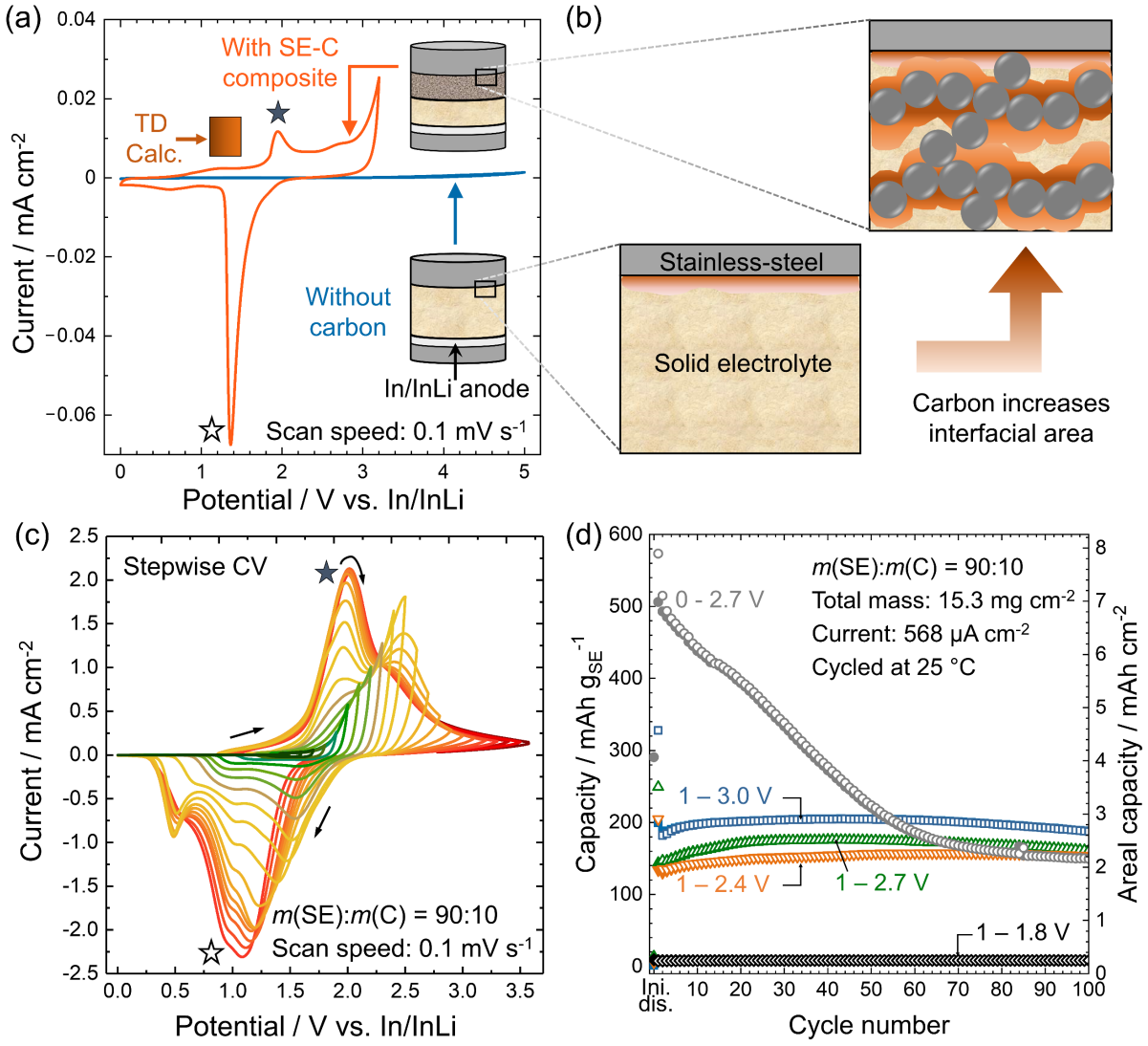

Figure 4: *(a) Cyclic voltammetry with (orange) and without (blue) compositing solid electrolyte with carbon (SE-C), as well as illustrations of the cell configurations.*[25] *The orange bar represents the theoretical stability window.*[24] *The enlarged schematics in (b) visualize the degree of degradation of electrolytes with and without carbon. (c) The oxidative stepwise CV with a SE-C composite displays that the peaks at ★ and ☆ are due to the redox activity of interphases. (d) The apparent redox behavior of SE-C composites is reversible with a sufficiently high lower-cutoff potential. The apparent capacities are normalized to the SE loading in the composite. Open and close symbols are charge and discharge capacity, respectively. Figures (c) and (d) are adapted with permission from reference 26. Copyright 2021 John Wiley and Sons.*

2.3. Tortuous and sluggish charge carrier transport and the transport-cyclability relationship

As the electrochemical reaction requires a sufficient supply of ion and electron, fast carrier transport in the composite is paramount for better cycling performance. While increasing the conducting media in the composite can facilitate the ion and electron supply, it sacrifices attainable energy density due to more inactive mass. Therefore, an optimization of the mixing ratio for the solid electrolyte and the conductive additive that enables the highest possible active material loading is needed. Figures 5a-b show a correlation between the cell cycling performance and volume fractions of ion- and electron-conducting phases with a model cathode composite. In this composite, Li_6PS_5Cl and carbon were mixed with volume fractions of ε(SE) and ε(C), respectively, while the active material and total cathode loading were kept constant. There is a clear optimum in terms of cell cyclability, as too small fraction of ion- or electron-conducting media in the composite is detrimental for battery performance. However, predicting the optimum mixing ratio is not trivial as it must correlate to the ion and electron transport in the composite. Systematic studies to better understand the charge carrier transport in the composite are inevitable.

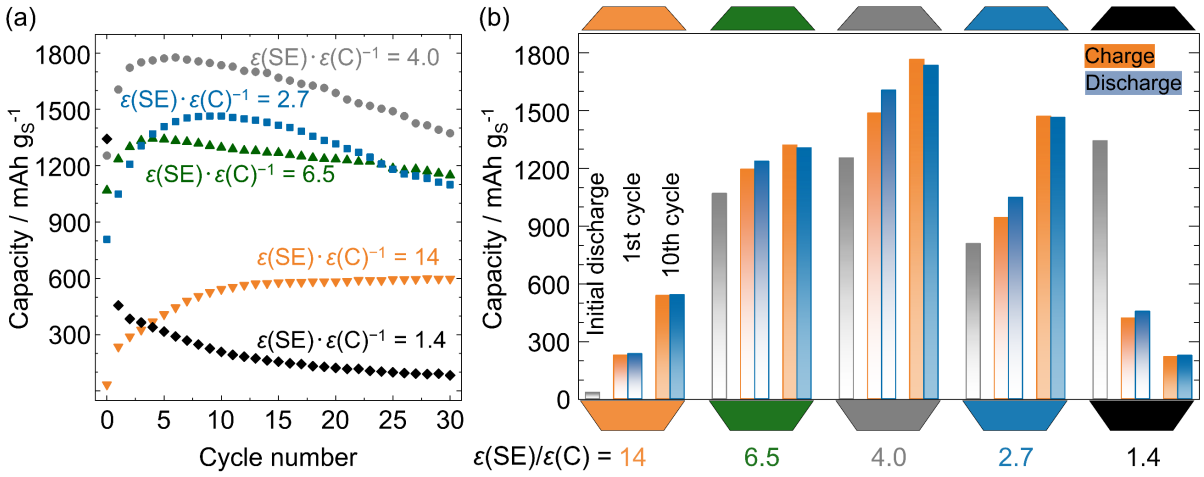

Figure 5: *(a) Cyclability of In/InLi|Li_6PS_5Cl|Li_6PS_5Cl-C-S cells with various Li_6PS_5Cl to C volume ratios $\varepsilon(SE)\cdot\varepsilon(C)^{-1}$ with fixed active material and total cathode loading (3.8 mg cm^{-2} and 12.7 mg cm^{-2}). (b) Bar plots of capacities at initial discharge, first cycle, and 10th cycle. Data digitized from reference 34. There is a clear optimum at around $\varepsilon(SE)\cdot\varepsilon(C)^{-1}$ = 4.0.*

2.3.1 Tortuous ionic conductivity

For a qualitative discussion of transport in solid-state battery composites, it is pivotal to introduce the effective ionic and electronic conductivities ($\sigma_{\text{ion}}^{\text{eff}}$ and $\sigma_{\text{e}}^{\text{eff}}$). These parameters are defined as $\sigma_k^{\text{eff}} = \frac{1}{R_k}\frac{d}{A}$, where R_k, d, and A are total ionic or electronic resistance (k is either ion or electron), total thickness of the composite and electrode area. Figure 6a summarizes the different configurations generally employed to assess the composite's effective conductivities. With the direct current (DC), R_{i} and R_{e} within the composite are measurable with the cell configurations (I) and (II), respectively. Under a small bias-voltage, the cell configuration (I) can block electrons, and only ions flow once the electrons are sufficiently polarized. By knowing interfacial resistances such as the resistance between the InLi anode and the solid electrolyte (SE), R_{i} can be obtained. As for cell configuration (II), ions are blocked at the steel electrodes, enabling the measurement of R_{e}.[26,34] In addition, cell configuration (III) can measure effective transport through impedance spectroscopy (with an alternating current, AC). These symmetric configurations help to eliminate unnecessary resistance contributions, other than the ones of interest.[35]

In solid-state Li-S batteries, the ion conduction in the composite is substantially tortuous and sluggish, as illustrated in Figure 6b, due to the ionically insulating components: carbon (C) and sulfur (S). Figure 6c shows the $\sigma_{\text{ion}}^{\text{eff}}$ of SE-C-S and SE-C composites as a function of a volume fraction of the solid electrolyte ε(SE). Here, $\sigma_{\text{ion}}^{\text{eff}}$ of SE-C-S composites (orange data) were measured by DC with the cell configuration (I), and that of SE-C composites (blue data) were by AC with cell configuration (III). The orange data are from the Li_6PS_5Cl-C-S composites identical to the ones in Figure 5. The blue data are from Li_6PS_5Cl-C composites to compare the additional influence of S on ionic transport. As for the SE-C composites, the spectra measured with impedance spectroscopy require a non-Faradaic transmission-line model (TLM) analysis, an approach to evaluate the effective conductivity in these porous electrodes (See Section 2.3.2 for details). In both composites, the $\sigma_{\text{ion}}^{\text{eff}}$ decreases over orders of magnitude when increasing contents of non-ion-conducting phases (S or C), *i.e.* a decreasing ε(SE). In other words, while the pure solid electrolyte exhibits fast ionic transport, this is no longer the case once it has been

implemented in a composite electrode.

The concept of tortuosity enables a quantitative description of the impact of insulating inclusions on transport in a complex microstructure.[36] In general, the $\sigma_{\text{ion}}^{\text{eff}}$ is related to the ionic conductivity in the undisturbed ion-conducting medium $\sigma_{\text{ion}}^{\text{SE}}$ by ε(SE) and tortuosity factor τ^2:

$$\sigma_{\text{ion}}^{\text{eff}} = \frac{\varepsilon(\text{SE})}{\tau^2}\sigma_{\text{ion}}^{\text{SE}}. \qquad \text{Eq. 4}$$

The tortuosity factor represents the effect of a microstructure of the composite on macroscopic transport. With the measured $\sigma_{\text{ion}}^{\text{eff}}$ and $\sigma_{\text{ion}}^{\text{SE}}$, as well as given ε(SE), the tortuosity factor τ^2 can be obtained as shown in Figure 6d. A robust approach to quantifying transport within a composite is effective medium theory, especially with the Bruggeman relation.[37] Although the original model was developed for homogeneously-dispersed spherical insulating inclusions in a conducting medium, the modified theorem with additional fitting parameters extends the model to more complex microstructures.[37] Within the model, the tortuosity factor to conducting volume relationship is given by

$$\tau^2 = \gamma \cdot \varepsilon(\text{SE})^{-\alpha}. \qquad \text{Eq. 5}$$

The original Bruggeman relation holds when $\gamma = 1$ and $\alpha = 0.5$. However, compared to the cathode composites data, a fit with these ideal values is far from the experimental data, shown with dashed curves in Figure 6c and d. Instead, the tortuosity factors from measurement results are well-fitted with $\gamma = 0.88$ and $\alpha = 4.77$ (solid curves in Figure 6c and d). This high value for α is very characteristic for well-mixed solid-state composites, as values less than three are typically obtained for cases of liquid electrolytes in the composite with $LiCoO_2$ or graphite.[38–40]

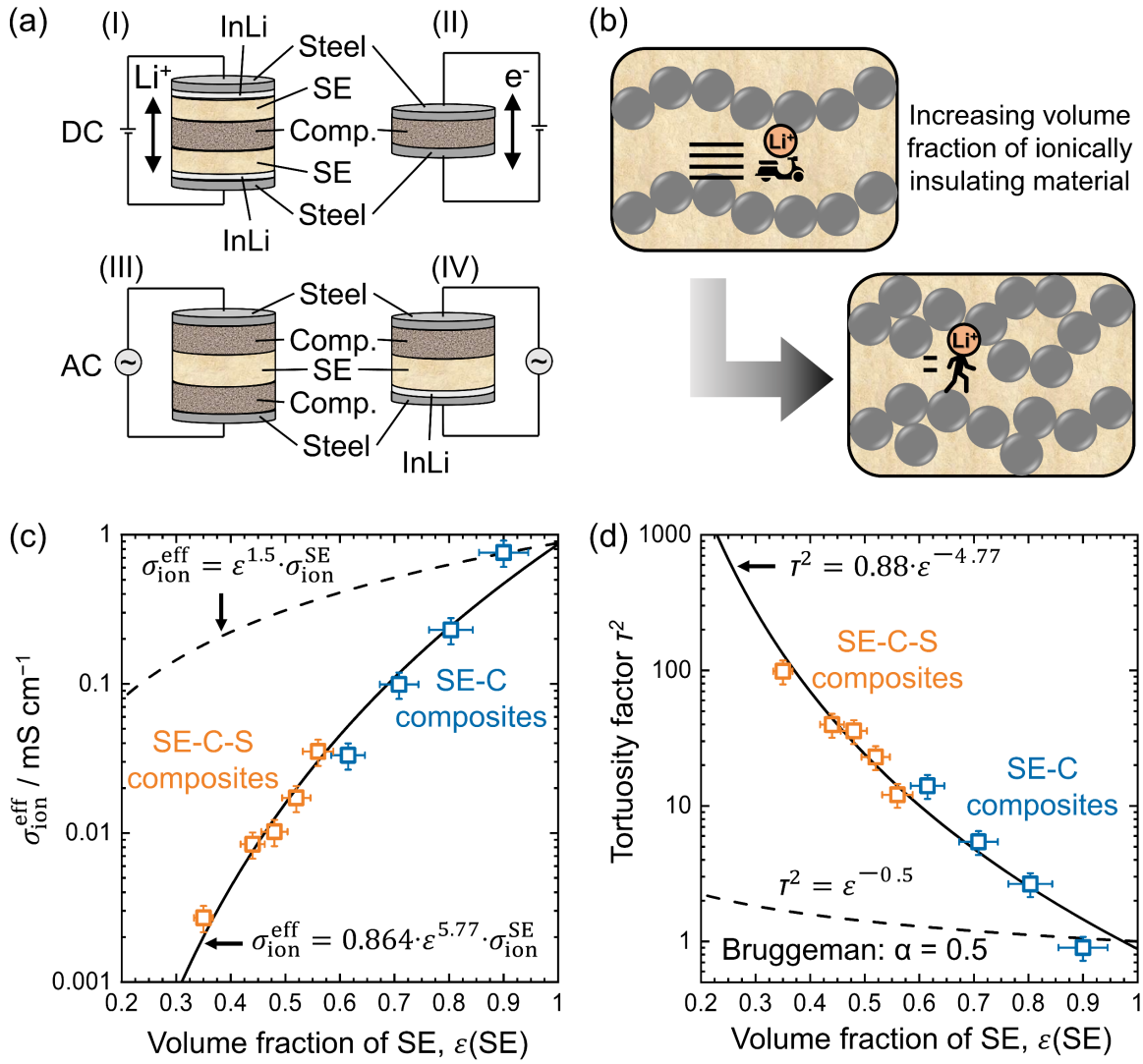

Figure 6: *(a) Cell configurations for various measurements. (I) and (II) are electron- and ion-blocking configurations for DC measurements. (III) Symmetric configuration for impedance spectroscopy and (IV) is for the potential-dependent impedance measurements with a In/InLi anode. The detail of (IV) will be discussed in Section 2.3.2. (b) Impact of increasing a fraction of non-ion-conducting phases. (c) The* σ_{ion}^{eff} *in various composites as a function of ε(SE). (d) Tortuosity factor from the measured effective conductivities and the conductivity of the pristine SE. The dashed and solid curves are with ideal and modified Bruggeman models. The data in (c) and (d) are digitized from ref 26 and 34. The error bars represent 20 % of error in conductivities*[41] *and 5 % in volume fractions.*

Clearly, ionic transport in composites consisting of sulfur, carbon and solid electrolytes is significantly tortuous. The slow conduction with a high tortuosity may simply arise from the microstructure, and two possible approaches of either using much faster solid ionic conductors or microstructural engineering can increase the effective transport. However, under operation conditions, there are other possible underlying influences. With a substantial interfacial area density, interfacial effects such as space-charge, defect accumulation, reaction with surface termination of carbon additives, and low percolation with disconnected conduction pathways, may become significant.

2.3.2 Linking ion transport in a composite to the electrolyte degradation and Li-S cell cycling performance

As shown above, the ionic transport in cathode composites is very sluggish and hampered, even before cycling. The cycling of composites leads to electrochemical degradation, further influencing transport. As discussed in Section 2.2, oxidative electrolyte degradation is unavoidable upon cycling solid-state Li-S batteries. Therefore, further investigation on the impact of degradation on the ionic conduction and cell cycling performance is required. However, the cell configuration (I) for the measurement of $\sigma_{\mathrm{ion}}^{\mathrm{eff}}$ through DC and the symmetric cell configuration (III) via AC impedance are not applicable for a potential-dependent measurement. Therefore, the cell configuration (IV) with an anode as a reference of the potential is needed to evaluate $\sigma_{\mathrm{ion}}^{\mathrm{eff}}$ as a function of the applied potential. We highlight that the cell configuration (IV) is not the only way for potential dependent measurement, and three- or four-electrode configurations with additional reference electrodes help for further developments, but it is technically challenging.[42] Since we employed InLi alloy as the anode for the following investigations, unless otherwise specified, the potentials hereafter are relative to the In/InLi (0 V vs. In/InLi is 0.62 V vs. Li^+/Li).[43] As briefly mentioned in the previous section, the obtained spectra were analyzed with a non-Faradaic TLM, which has been typically employed to study ion transport in the liquid electrolyte immersed in the electrode porous microstructure, and its application has recently been expanded to the solid-state battery researches.[39,44–46] We emphasize that the non-Faradaic TLM assumes no charge

transfer and, despite the very similar resulting mathematical expression, it is fundamentally different from the model based on the charge transfer and diffusion in the active materials. Although the impedance spectra from the cells with sulfur cathodes typically possess Nyquist plot with a straight line at a 45° angle for low frequencies that often fit with the Randles equivalent circuit, the physically meaningful equivalent circuit may be different in some cases. Recent solid-state Li-S battery studies have mainly focused on improving the charge-transfer and charge-carrier diffusion in the active material. While there is no doubt about its importance, a substantial cell resistance may also arise from the ion transport through the tortuous solid electrolyte in composites with a substantial interfacial area, which tends to be overlooked but is equally important, as discussed in Section 2.3.1. Here we want to refer the readers to our recent work, which entails the detailed confirmation of the validity and applicability of the TLMs, the applied equivalent circuit, and mathematical formulations.[26] As a side note, the widespread semi-circle approach overestimates $\sigma_{\text{ion}}^{\text{eff}}$ by at least a factor of three in theory. This leads to misunderstanding the transport limitations in composites when substantial interfacial capacitances are at play, as is the case in the cathode composites for solid-state Li-S batteries.[47]

In order to link the solid electrolyte degradation to the resulting effective ion transport in these composites, the potential-dependent ion-transport measurement has been demonstrated with a model Li_6PS_5Cl-C composite, same as the one in Figure 4d.[26] Identical cells with cell configuration (IV) were employed for oxidative and reductive tests in Figure 7a. The potential on the cathode side was slowly swept from OCV (~1.55 V vs. In/InLi) to the target potential (1.6 V and 1.4 V for the oxidative and reductive tests, respectively) and kept for 12 h to let the degradation proceed, followed by one hour of relaxation before the impedance measurement. As an indicator of the onset and degree of degradation, the consumed or delivered apparent capacities during the sweep, and hold, of the potential were measured as the cumulative charge shown in Figure 7a. While the thermodynamic calculation predicts the stability window of Li_6PS_5Cl to be between 1.1 – 1.4 V (orange bar in the bottom panel), a wider experimental electrochemical stability window of 0.7 – 1.7 V can be observed (green-shaded region). Despite the limited potential range for TLM analysis due to the appearance of an additional process

overlapping with the frequency region of interest, there is a clear voltage window maintaining the $\sigma_{\text{ion}}^{\text{eff}}$ at a constant value (blue-shaded in Figure 7a). This range can be referred to as a "*stability window of good effective ion-transport*" for a given condition summarized in the bottom panel in Figure 7a. It is evident that a small gap between the onset potential of the oxidative solid electrolyte degradation and the upper-threshold potential for high $\sigma_{\text{ion}}^{\text{eff}}$ exists (1.7 V and 2.0 V, respectively). This gap may indicate the formation of ionically conductive interphases, *e.g.* amorphous Li-thiophosphates, and opens the possibility to utilize the reversible apparent redox capacity of solid electrolytes to boost the attainable capacity of solid-state Li-S batteries without detrimentally affecting the overall ionic transport.

Indeed, the so-called "activation behavior" in which the capacity increases upon cycling is seen in the initial cycles when the SE-C-S composite is cycled with various cutoff potentials (Figure 7b). The activation behavior is most likely due to the formation and the redox activity of the interphases and a clear correlation between the highest observed capacity, the magnitude of activation, the overpotential after long-term cycling, and the capacity retention, is seen in Figure 7b-d. The highest capacity of over 2100 mAh g_S^{-1} is delivered with the cell discharged down to 0 V, which is higher than the theoretical capacity of sulfur (1672 mAh g_S^{-1}). Hence it is evident that there is a substantial contribution from the solid electrolyte degradation and redox activity of formed interphases. However, the capacity retention is very poor with such a substantial reductive degradation, as also seen with the SE-C composite (Figure 4d). In contrast, the cells cycled with a fixed lower-cutoff potential of 1.0 V exhibit much better capacity retention with a little activation. Cycling up to 2.7 V shows a superior cyclability to the one cycled up to 3.0 V, leading to the areal capacity of about 4.6 mAh cm^{-2} at the 50^{th} cycle. The critical difference is seen in the overpotential at the 50^{th} cycle, where the cell cycled with the upper cutoff of 3.0 V has an overpotential significantly higher than the one cycled with 2.7 V. The cycling data corroborate that even more sluggish transport results from more intense oxidative degradation, which deteriorates the cell cyclability (Figure 7c). Overall, these findings highlight the importance to carefully explore the relationship between practical electrolyte stability, the impact of electrolyte degradation on effective transport, and the resulting cell cycling performance.

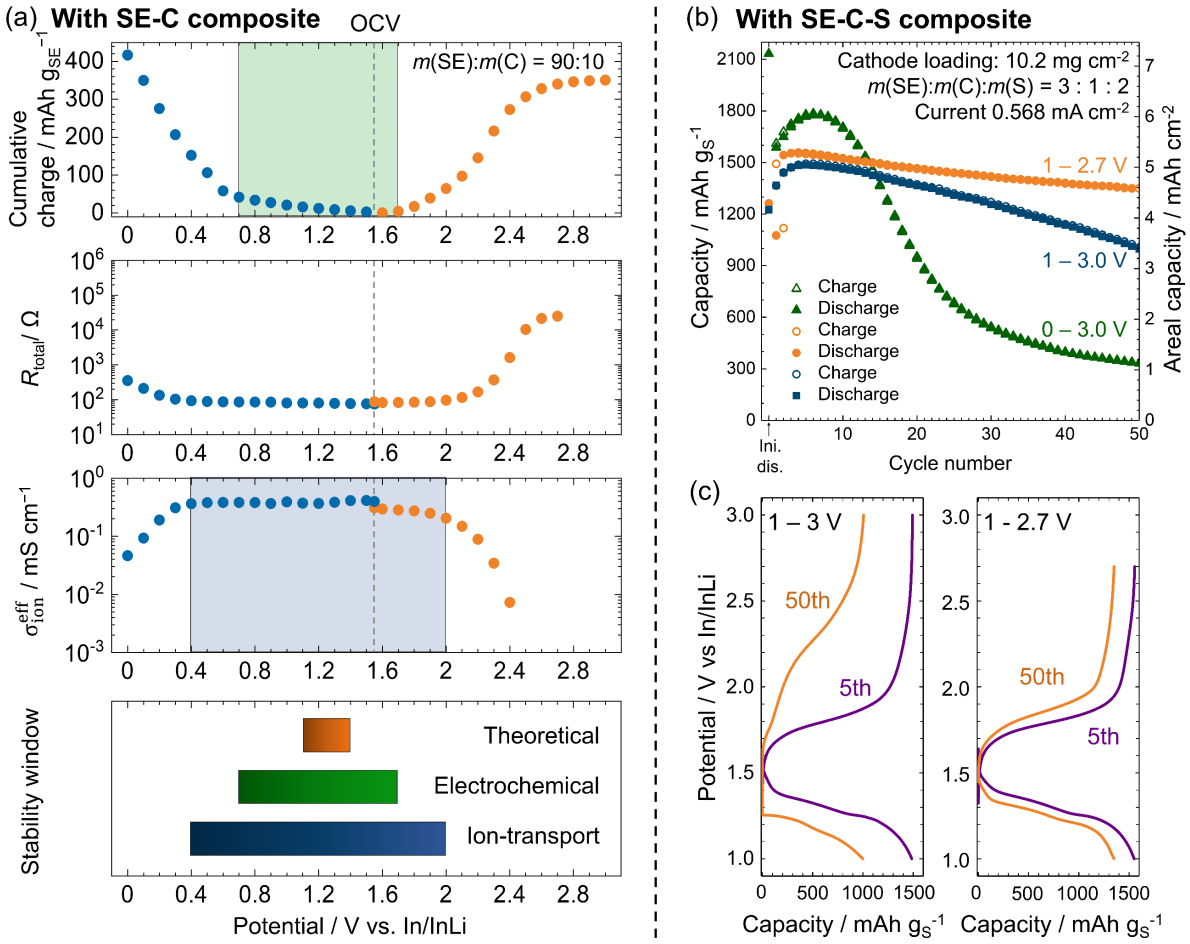

Figure 7: *The cumulative charge, the total cell resistance R_{total}, and the extracted σ_{ion}^{eff} in the Li_6PS_5Cl-C composite cathode are shown in (a) as a function of applied potential. The green shade shows the experimental electrochemical stability window, and the blue shade shows the stability window of good effective ion transport. The bottom panel summarizes the three different types of stability windows: the theoretically-predicted electrochemical stability window (orange), the electrochemical stability windows based on the monitored cumulative charge (green), and the stability window determined by the effective ion-transport in the composite (blue). (b) The cycling performances of solid-state Li-S cells with the Li_6PS_5Cl-C-S composite. The panel (c) shows the potential profiles of cells cycled between 1 – 2.7 V and 1 – 3.0 V at 5th and 50th cycles, revealing a more significant evolution in the overpotential in the cell with the upper-cutoff potential of 3.0 V. Figures are adapted with permission from reference* 26. *Copyright 2021 John Wiley and Sons.*

3. Summary and perspectives

To visualize the road from the current cell performance to the practical solid-state Li-S batteries, the gravimetric energy densities of hypothetical cells achievable after overcoming specific challenges are summarized in Figure 8. The details of energy density calculations and utilized parameters are described and tabulated in Figure S1 and Table S1 (Supporting Information). The gravimetric energy density of the In/InLi|Li_6PS_5Cl|Li_6PS_5Cl-C-S cell shown in Figure 7b achieves about 36 Wh kg^{-1}. The here-estimated specific energy includes the mass of current collectors, but the mass of the cell packings, tabs, and binders are excluded. The employment of a lithium-metal anode and a thin layer of a solid separator will significantly enhance the solid-state battery performance,[13,14,48] reaching the specific energy of 417 Wh kg^{-1}. Notably, this value is attainable without any modification on the cathode side, highlighting a promising performance of a high-capacity conversion-type cathode. The possibility of employing a thin separator layer (~30 μm) and a lithium-metal anode has successfully been demonstrated with Li_6PS_5Cl and the intercalation-type cathode active materials very recently.[49] Another scenario with a different layer thickness (100 μm) is also showcased in Table S2 (Supporting Information).

For further enhancement, two strategies, both requiring faster transport in the composite cathode, can be considered: (1) to enlarge a layer thickness of the cathode and (2) to increase the weight fraction of sulfur in the composite. The gravimetric energy density of the hypothetical cell can achieve over 800 Wh kg^{-1} if one assumes unchanged average discharge potentials. To meet this requirement, it is clear that further improvement of ion transport in the cathode composite is mandatory. The resistance of the cathode layer will increase by a factor of three through loading three times the amount of cathode composite. Furthermore, increasing the weight fraction of sulfur in the composite from 33 % to 45 % reduces the $\sigma_{\mathrm{ion}}^{\mathrm{eff}}$ from 0.006 mS cm^{-1} to 0.002 mS cm^{-1} based on the data in Figure 6c. Thus, the total resistance increase becomes close to an order of magnitude. The required current density for 0.1 C also increases by about a factor of four, and hence, to maintain the average discharge potentials, faster effective ion transport is required. Overall, the following conclusions and perspectives can be drawn.

1) To secure the fast ion transport within a thick composite cathode layer, the exploration of fast-

conduction solid electrolytes is inevitable. The here-proposed roadmap demands almost 40 times higher effective ionic conductivity, meaning a generally accepted metric of 1 mS cm^{-1} being practical, needs to be reconsidered for solid-state Li-S batteries. In fact, recent theoretical work suggests that for solid state batteries with intercalation-type cathode active materials ionic conductivities of at least 10 mS cm^{-1} are needed.[50] Considering that solid-state Li-S batteries contain even more ionically insulating materials, even higher needed ionic conductivities seem likely. Despite the other difficulties, e.g., stability, processibility, and chemical compatibility, some sodium ion conducting solids possess substantially high conductivities,[51,52] which may allow the use of sulfur composite cathodes. Nevertheless, the fact that only a few solid electrolytes achieve the ionic conductivity of higher than 10 mS cm^{-1} greatly motivates further exploration.

2) While the chemo-mechanical failure becomes less intense by well-compositing the cathode components, the enhanced interfacial area magnifies the impact of electrolyte degradation. This dilemma calls for the exploration of electrolytes that do not drastically lose ionic conductivity upon processing and cycling. Mechanically soft and electrochemically stable electrolytes within the potential window of the sulfur redox activity need to be developed. Among the various emerging lithium-conducting solids, halide-based materials and variants of *closo*-borates are the two new classes of promising solid electrolytes besides the sulfide-based materials.[53–56]

3) Despite the low effective ionic conductivity in the current composite, the ion supply may become faster by reducing "traveling distances" through nano- and micro-structural designs of the cathode composite. Establishing the highly conductive "highways" for lithium ions facilitates fast ion transport within composites. Unlike liquids, no separator is needed to combine different solid electrolytes, enabling the employment of the right electrolyte at the right place. Although the chemical compatibility needs to be examined, utilizing the highly-conducting solid electrolytes as "highways" and the highly stable solid electrolytes as "driveways" to secure the local ion supply may reduce the impact of interfacial degradation. The species of employed carbons, the microstructure of conductive additives and their loading fractions expand the options for further

interface engineering.

4) Battery operation at elevated temperature may be an apparent strategy to overcome the transport limitation in the cathode composite. Operation at elevated temperature further paves the way for achieving the high current density required for charging and discharging high-capacity sulfur cathodes with lithium metal.[57] In contrast, the behavior of the kinetically stabilized interface with substantially high interfacial area density inside the cathode composite during battery operation at high temperatures is still not well understood. Further investigation of the temperature effect is inevitable for practical applications.

There are additional approaches, as well as challenges, towards practical solid-state Li-S batteries. For instance, halogens or selenium incorporation into the active materials can improve the ion or electron conduction and enhance cyclability.[58,59] Employing metal sulfides instead of pure sulfur may help to reduce the loading of electron conductive additives.[60,61] Various mixing processing, *e.g.* liquid-phase and gas-phase mixing techniques in addition to mechanical milling, may help to establish intimate contact among the cathode components.[62] The cost effectiveness, scalability of materials, processing procedures, and the weight of the cell containers are also vital factors for commercial applications.[63] Additionally, binder inclusion and modification, as well as the decrease of the necessary applied pressures, may further complicate the charge transfer and carrier conduction. Nevertheless, monitoring the transport in the composite and analyses through effective conductivities is paramount for a quantitative discussion to further improve solid-state Li-S batteries. A steady improvement of the cathode composite will pave the way for the practical solid-state Li-S batteries in the coming years.

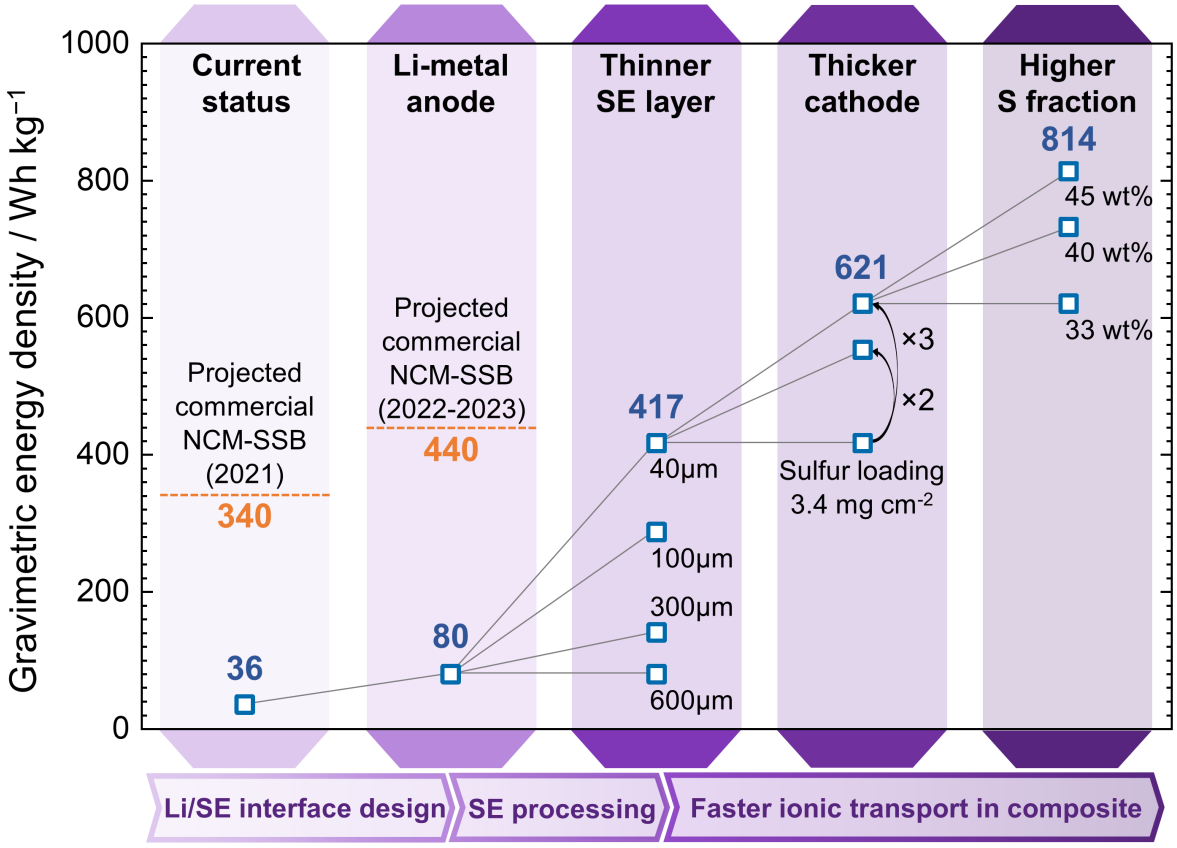

Figure 8: *Roadmap toward the practical solid-state Li-S batteries from the currently reported cell performance. The start-line corresponds to the cell shown in Figure 7b with the specific capacity of 1450 mAh* g_S^{-1}*, the average discharge voltage of 1.29 V vs In/InLi, the mass ratio of SE, C and S of 3:1:2, the total cathode loading of 10.2 mg* cm^{-2}*, and the total cell weight of 178.0 mg* cm^{-2}*. Through overcoming specific challenges, the predicted performance of the hypothetical solid-state Li-S batteries with parameters goes beyond 800 Wh* kg^{-1}*. Note that all calculations include current collectors. Projected commercial cell data are from* [64].

■ Biographies

Saneyuki Ohno received his B. Eng. in Applied Physics from Keio University in 2012 and his Ph.D. in Materials Science from California Institute of Technology in 2017. Following the postdoctoral research at the Justus Liebig University Giessen with Humboldt research fellowship, he joined the Department of Applied Chemistry at Kyushu University as an Assistant Professor in 2020. His research interests

include functional inorganic materials and composites with ion/electron/phonon transport for energy storage and conversion, e.g., solid electrolytes, thermoelectrics, and electrodes for solid-state batteries.

Wolfgang Zeier received his doctorate from the University of Mainz in 2013, followed by postdoctoral stays at the University of Southern California, the California Institute of Technology and Northwestern University. After leading an independent research group at the University of Giessen, he now holds a professorship for inorganic solid-state chemistry at the University of Muenster. In addition, he heads a department at the Helmholtz-Institute Münster, Ionics in Energy Storage. His research interests encompass the fundamental structure-property relationships in solids, with a focus on thermoelectric and ion-conducting materials, as well as solid-solid interfacial chemistry for all-solid-state batteries.

Supporting Information

The Supporting information is available free of charge.

The numberings of the hypothetical cells in Figure 8, corresponding parameters utilized for the gravimetric energy calculations, and energy density with another scenario with SE layer thickness of 100 µm.

■ AUTHOR INFORMATION

Corresponding Authors
Saneyuki Ohno
Wolfgang G. Zeier

Notes

The authors declare no competing financial interest.

■ ACKNOWLEDGMENTS

The research led to this work was supported by the Federal Ministry of Education and Research (BMBF) within the project LISZUBA under grant number of 03XP0115A. S.O. acknowledges financial support from the JSPS KAKENHI Grant Number JP 21K14720.

■ REFERENCES

(1) Bhargav, A.; He, J.; Gupta, A.; Manthiram, A. Lithium-Sulfur Batteries: Attaining the Critical Metrics. *Joule* **2020**, *4*, 285–291.

(2) Bruce, P. G.; Freunberger, S. A.; Hardwick, L. J.; Tarascon, J.-M. Li–O_2 and Li–S Batteries with High Energy Storage. *Nat. Mater.* **2012**, *11*, 19–29.

(3) Herbert, D.; Ulam, J. *United States Patent Office l 3,043,896 ELECTRIC DRY CELLS AND STORAGE BATTERES*; 1958.

(4) Mikhaylik, Y. V.; Akridge, J. R. Polysulfide Shuttle Study in the Li/S Battery System. *J. Electrochem. Soc.* **2004**, *151*, A1969-A1976.

(5) Fang, R.; Zhao, S.; Sun, Z.; Wang, D. W.; Cheng, H. M.; Li, F. More Reliable Lithium-Sulfur Batteries: Status, Solutions and Prospects. *Adv. Mater.* **2017**, *29*, 1606823.

(6) Janek, J.; Zeier, W. G. A Solid Future for Battery Development. *Nat. Energy* **2016**, *1*, 16141.

(7) Muy, S.; Bachman, J. C.; Giordano, L.; Chang, H. H.; Abernathy, D. L.; Bansal, D.; Delaire, O.; Hori, S.; Kanno, R.; Maglia, F.; Lupart, S.; Lamp, P.; Shao-Horn, Y. Tuning Mobility and Stability of Lithium Ion Conductors Based on Lattice Dynamics. *Energy Environ. Sci.* **2018**, *11*, 850–859.

(8) Sakuda, A.; Hayashi, A.; Tatsumisago, M. Sulfide Solid Electrolyte with Favorable Mechanical Property for All-Solid-State Lithium Battery. *Sci. Rep.* **2013**, *3*, 2261.

(9) Ohno, S.; Banik, A.; Dewald, G. F.; Kraft, M. A.; Krauskopf, T.; Minafra, N.; Till, P.; Weiss, M.; Zeier, W. G. Materials Design of Ionic Conductors for Solid State Batteries. *Prog. Energy* **2020**, *2*, 022001.

(10) Culver, S. P.; Koerver, R.; Krauskopf, T.; Zeier, W. G. Designing Ionic Conductors: The Interplay between Structural Phenomena and Interfaces in Thiophosphate-Based Solid-State Batteries. *Chem. Mater.* **2018**, *30*, 4179–4192.

(11) Ghidiu, M.; Ruhl, J.; Culver, S. P.; Zeier, W. G.; Culver, P.; Zeier, W. G. Solution-Based Synthesis of Lithium Thiophosphate Superionic Conductors for Solid-State Batteries: A Chemistry Perspective. *J. Mater. Chem. A* **2019**, *7*, 17735–17753.

(12) Banik, A.; Famprikis, T.; Ghidiu, M.; Ohno, S.; Kraft, M. A.; Zeier, W. G. On the Underestimated Influence of Synthetic Conditions in Solid Ionic Conductors. *Chem. Sci.* **2021**, *12*, 6238–6263.

(13) Hatzell, K. B.; Chen, X. C.; Cobb, C. L.; Dasgupta, N. P.; Dixit, M. B.; Marbella, L. E.; McDowell, M. T.; Mukherjee, P. P.; Verma, A.; Viswanathan, V.; Westover, A. S.; Zeier, W. G. Challenges in Lithium Metal Anodes for Solid-State Batteries. *ACS Energy Lett.* **2020**, *5*, 922–934.

(14) Krauskopf, T.; Richter, F. H.; Zeier, W. G.; Janek, J. Physicochemical Concepts of the Lithium Metal Anode in Solid-State Batteries. *Chem. Rev.* **2020**, *120*, 7745–7794.

(15) Koerver, R.; Walther, F.; Aygün, I.; Sann, J.; Dietrich, C.; Zeier, W. G.; Janek, J. Redox-Active Cathode Interphases in Solid-State Batteries. *J. Mater. Chem. A* **2017**, *5*, 22750–22760.

(16) Koerver, R.; Zhang, W.; De Biasi, L.; Schweidler, S.; Kondrakov, A. O.; Kolling, S.; Brezesinski, T.; Hartmann, P.; Zeier, W. G.; Janek, J. Chemo-Mechanical Expansion of Lithium Electrode Materials-on the Route to Mechanically Optimized All-Solid-State Batteries. *Energy Environ. Sci.* **2018**, *11*, 2142–2158.

(17) Ohno, S.; Koerver, R.; Dewald, G.; Rosenbach, C.; Titscher, P.; Steckermeier, D.; Kwade, A.; Janek, J. J.; Zeier, W. G. Observation of Chemomechanical Failure and the Influence of Cutoff Potentials in All-Solid-

State Li-S Batteries. *Chem. Mater.* **2019**, *31*, 2930–2940.

(18) Chen, M.; Adams, S. High Performance All-Solid-State Lithium/Sulfur Batteries Using Lithium Argyrodite Electrolyte. *J. Solid State Electrochem.* **2015**, *19*, 697–702.

(19) Schlem, R.; Burmeister, C. F.; Michalowski, P.; Ohno, S.; Dewald, G. F.; Kwade, A.; Zeier, W. G. Energy Storage Materials for Solid-State Batteries: Design by Mechanochemistry. *Adv. Energy Mater.* **2021**, 2101022. https://doi.org/10.1002/aenm.202101022.

(20) Gritzner, G.; Kreysa, G. Nomenclature, Symbols and Definitions in Electrochemical Engineering (IUPAC Recommendations 1993). *Pure Appl. Chem.* **1993**, *65*, 1009–1020.

(21) Zhang, W.; Leichtweiß, T.; Culver, S. P.; Koerver, R.; Das, D.; Weber, D. A.; Zeier, W. G.; Janek, J. The Detrimental Effects of Carbon Additives in $Li_{10}GeP_2S_{12}$-Based Solid-State Batteries. *ACS Appl. Mater. Interfaces* **2017**, *9*, 35888–35896.

(22) Schwietert, T. K.; Arszelewska, V. A.; Wang, C.; Yu, C.; Vasileiadis, A.; de Klerk, N. J. J.; Hageman, J.; Hupfer, T.; Kerkamm, I.; Xu, Y.; van der Maas, E.; Kelder, E. M.; Ganapathy, S.; Wagemaker, M. Clarifying the Relationship between Redox Activity and Electrochemical Stability in Solid Electrolytes. *Nat. Mater.* **2020**, *19*, 428–435.

(23) Walther, F.; Koerver, R.; Fuchs, T.; Ohno, S.; Sann, J.; Rohnke, M.; Zeier, W. G.; Janek, J. J. Visualization of the Interfacial Decomposition of Composite Cathodes in Argyrodite-Based All-Solid-State Batteries Using Time-of-Flight Secondary-Ion Mass Spectrometry. *Chem. Mater.* **2019**, *31*, 3745–3755.

(24) Zhu, Y.; He, X.; Mo, Y. Origin of Outstanding Stability in the Lithium Solid Electrolyte Materials: Insights from Thermodynamic Analyses Based on First-Principles Calculations. *ACS Appl. Mater. Interfaces* **2015**, *7*, 23685–23693.

(25) Dewald, G. F.; Ohno, S.; Kraft, M. A.; Koerver, R.; Till, P.; Vargas-Barbosa, N. M.; Janek, J.; Zeier, W. G. Experimental Assessment of the Practical Oxidative Stability of Lithium Thiophosphate Solid Electrolytes. *Chem. Mater.* **2019**, *31*, 8328–8337.

(26) Ohno, S.; Rosenbach, C.; Dewald, G. F.; Janek, J.; Zeier, W. G. Linking Solid Electrolyte Degradation to Charge Carrier Transport in the Thiophosphate-Based Composite Cathode toward Solid-State Lithium-Sulfur Batteries. *Adv. Funct. Mater.* **2021**, *31*, 2010620.

(27) Walther, F.; Randau, S.; Schneider, Y.; Sann, J.; Rohnke, M.; Richter, F. H.; Zeier, W. G.; Janek, J. Influence of Carbon Additives on the Decomposition Pathways in Cathodes of Lithium Thiophosphate-Based All-Solid-State Batteries. *Chem. Mater.* **2020**, *32*, 6123–6136.

(28) Tan, D. H. S.; Wu, E. A.; Nguyen, H.; Chen, Z.; Marple, M. A. T.; Doux, J. M.; Wang, X.; Yang, H.; Banerjee, A.; Meng, Y. S. Elucidating Reversible Electrochemical Redox of Li_6PS_5Cl Solid Electrolyte. *ACS Energy Lett.* **2019**, *4*, 2418–2427.

(29) Hakari, T.; Nagao, M.; Hayashi, A.; Tatsumisago, M. Preparation of Composite Electrode with Li_2S-P_2S_5 Glasses as Active Materials for All-Solid-State Lithium Secondary Batteries. *Solid State Ionics* **2014**, *262*, 147–150.

(30) Wang, S.; Tang, M.; Zhang, Q.; Li, B.; Ohno, S.; Walther, F.; Pan, R.; Xu, X.; Xin, C.; Zhang, W.; Li, L.; Shen, Y.; Richter, F. H.; Janek, J.; Nan, C.-W. Lithium Argyrodite as Solid Electrolyte and Cathode Precursor for Solid-State Batteries with Long Cycle Life. *Adv. Energy Mater.* **2021**, 2101370.

https://doi.org/10.1002/aenm.202101370.

(31) Han, F.; Zhu, Y.; He, X.; Mo, Y.; Wang, C. Electrochemical Stability of $Li_{10}GeP_2S_{12}$ and $Li_7La_3Zr_2O_{12}$ Solid Electrolytes . *Adv. Energy Mater.* **2016**, *6*, 1501590.

(32) Yu, C.; Hageman, J.; Ganapathy, S.; Van Eijck, L.; Zhang, L.; Adair, K. R.; Sun, X.; Wagemaker, M. Tailoring Li_6PS_5Br Ionic Conductivity and Understanding of Its Role in Cathode Mixtures for High Performance All-Solid-State Li-S Batteries. *J. Mater. Chem. A* **2019**, *7*, 10412–10421.

(33) Swamy, T.; Chen, X.; Chiang, Y. M. Electrochemical Redox Behavior of Li Ion Conducting Sulfide Solid Electrolytes. *Chem. Mater.* **2019**, *31*, 707–713.

(34) Dewald, G. F.; Ohno, S.; Hering, J. G. C.; Janek, J.; Zeier, W. G. Analysis of Charge Carrier Transport Toward Optimized Cathode Composites for All-Solid-State Li−S Batteries. *Batter. Supercaps* **2021**, *4*, 183–194.

(35) Kaiser, N.; Spannenberger, S.; Schmitt, M.; Cronau, M.; Kato, Y.; Roling, B. Ion Transport Limitations in All-Solid-State Lithium Battery Electrodes Containing a Sulfide-Based Electrolyte. *J. Power Sources* **2018**, *396*, 175–181.

(36) Bruggeman, D. A. G. Berechnung Verschiedener Physikalischer Konstanten von Heterogenen Substanzen. I. Dielektrizitätskonstanten Und Leitfähigkeiten Der Mischkörper Aus Isotropen Substanzen. *Ann. Phys.* **1935**, *416*, 636–664.

(37) Tjaden, B.; Cooper, S. J.; Brett, D. J.; Kramer, D.; Shearing, P. R. On the Origin and Application of the Bruggeman Correlation for Analysing Transport Phenomena in Electrochemical Systems. *Curr. Opin. Chem. Eng.* **2016**, *12*, 44–51.

(38) Ebner, M.; Chung, D. W.; García, R. E.; Wood, V. Tortuosity Anisotropy in Lithium-Ion Battery Electrodes. *Adv. Energy Mater.* **2014**, *4*, 1–6.

(39) Landesfeind, J.; Hattendorff, J.; Ehrl, A.; Wall, W. A.; Gasteiger, H. A. Tortuosity Determination of Battery Electrodes and Separators by Impedance Spectroscopy. *J. Electrochem. Soc.* **2016**, *163*, A1373–A1387.

(40) Usseglio-Viretta, F. L. E.; Colclasure, A.; Mistry, A. N.; Claver, K. P. Y.; Pouraghajan, F.; Finegan, D. P.; Heenan, T. M. M.; Abraham, D.; Mukherjee, P. P.; Wheeler, D.; Shearing, P.; Cooper, S. J.; Smith, K. Resolving the Discrepancy in Tortuosity Factor Estimation for Li-Ion Battery Electrodes through Micro-Macro Modeling and Experiment. *J. Electrochem. Soc.* **2018**, *165*, A3403–A3426.

(41) Ohno, S.; Bernges, T.; Buchheim, J.; Duchardt, M.; Hatz, A. K.; Kraft, M. A.; Kwak, H.; Santhosha, A. L.; Liu, Z.; Minafra, N.; Tsuji, F.; Sakuda, A.; Schlem, R.; Xiong, S.; Zhang, Z.; Adelhelm, P.; Chen, H.; Hayashi, A.; Jung, Y. S.; Lotsch, B. V.; Roling, B.; Vargas-Barbosa, N. M.; Zeier, W. G. How Certain Are the Reported Ionic Conductivities of Thiophosphate-Based Solid Electrolytes? An Interlaboratory Study. *ACS Energy Lett.* **2020**, *5*, 910–915.

(42) Simon, F. J.; Hanauer, M.; Henss, A.; Richter, F. H.; Janek, J. Properties of the Interphase Formed between Argyrodite-Type Li_6PS_5Cl and Polymer-Based PEO_{10}:LiTFSI. *ACS Appl. Mater. Interfaces* **2019**, *11*, 42186–42196.

(43) Santhosha, A. L.; Medenbach, L.; Buchheim, J. R.; Adelhelm, P. The Indium-Lithium Electrode in Solid-State Lithium Ion Batteries: Phase Formation, Redox Potentials and Interface Stability. *Batter. Supercaps* **2019**, *2*, 524–529.

(44) Ogihara, N.; Itou, Y.; Kawauchi, S. Ion Transport in Porous Electrodes Obtained by Impedance Using a Symmetric Cell with Predictable Low-Temperature Battery Performance. *J. Phys. Chem. Lett.* **2019**, *10*, 5013–5018.

(45) Usseglio-Viretta, F. L. E.; Mai, W.; Colclasure, A. M.; Doeff, M.; Yi, E.; Smith, K. Enabling Fast Charging of Lithium-Ion Batteries through Secondary- /Dual- Pore Network: Part I - Analytical Diffusion Model. *Electrochim. Acta* **2020**, *342*, 136034.

(46) Minnmann, P.; Quillman, L.; Burkhardt, S.; Richter, F. H.; Janek, J. Editors' Choice—Quantifying the Impact of Charge Transport Bottlenecks in Composite Cathodes of All-Solid-State Batteries. *J. Electrochem. Soc.* **2021**, *168*, 040537.

(47) Barsoukov, E.; Macdonald, J. R. *Impedance Spectroscopy: Theory, Experiment, and Applications*; 2005.

(48) Randau, S.; Weber, D. A.; Kötz, O.; Koerver, R.; Braun, P.; Weber, A.; Ivers-Tiffée, E.; Adermann, T.; Kulisch, J.; Zeier, W. G.; Richter, F. H.; Janek, J. Benchmarking the Performance of All-Solid-State Lithium Batteries. *Nat. Energy* **2020**, *5*, 259–270.

(49) Lee, Y. G.; Fujiki, S.; Jung, C.; Suzuki, N.; Yashiro, N.; Omoda, R.; Ko, D. S.; Shiratsuchi, T.; Sugimoto, T.; Ryu, S.; Ku, J. H.; Watanabe, T.; Park, Y.; Aihara, Y.; Im, D.; Han, I. T. High-Energy Long-Cycling All-Solid-State Lithium Metal Batteries Enabled by Silver–Carbon Composite Anodes. *Nat. Energy* **2020**, *5*, 299–308.

(50) Bielefeld, A.; Weber, D. A.; Janek, J. Modeling Effective Ionic Conductivity and Binder Influence in Composite Cathodes for All-Solid-State Batteries. *ACS Appl. Mater. Interfaces* **2020**, *12*, 12821–12833.

(51) Hayashi, A.; Masuzawa, N.; Yubuchi, S.; Tsuji, F.; Hotehama, C.; Sakuda, A.; Tatsumisago, M. A Sodium-Ion Sulfide Solid Electrolyte with Unprecedented Conductivity at Room Temperature. *Nat. Commun. 2019 101* **2019**, *10*, 1–6.

(52) Tang, W. S.; Yoshida, K.; Soloninin, A. V.; Skoryunov, R. V.; Babanova, O. A.; Skripov, A. V.; Dimitrievska, M.; Stavila, V.; Orimo, S. I.; Udovic, T. J. Stabilizing Superionic-Conducting Structures via Mixed-Anion Solid Solutions of Monocarba-Closo-Borate Salts. *ACS Energy Lett.* **2016**, *1*, 659–664.

(53) Muy, S.; Voss, J.; Schlem, R.; Koerver, R.; Sedlmaier, S. J.; Maglia, F.; Lamp, P.; Zeier, W. G.; Shao-Horn, Y. High-Throughput Screening of Solid-State Li-Ion Conductors Using Lattice-Dynamics Descriptors. *iScience* **2019**, *16*, 270–282.

(54) Duchêne, L.; Remhof, A.; Hagemann, H.; Battaglia, C. Status and Prospects of Hydroborate Electrolytes for All-Solid-State Batteries. *Energy Storage Mater.* **2020**, *25*, 782-794.

(55) Kim, S.; Oguchi, H.; Toyama, N.; Sato, T.; Takagi, S.; Otomo, T.; Arunkumar, D.; Kuwata, N.; Kawamura, J.; Orimo, S. ichi. A Complex Hydride Lithium Superionic Conductor for High-Energy-Density All-Solid-State Lithium Metal Batteries. *Nat. Commun.* **2019**, *10*, 1081.

(56) Riegger, L. M.; Schlem, R.; Sann, J.; Zeier, W. G.; Janek, J. Lithium-Metal Anode Instability of the Superionic Halide Solid Electrolytes and the Implications for Solid-State Batteries. *Angew. Chemie Int. Ed.* **2021**, *60*, 6718–6723.

(57) Jolly, D. S.; Ning, Z.; Hartley, G. O.; Liu, B.; Melvin, D. L. R.; Adamson, P.; Marrow, J.; Bruce, P. G. Temperature Dependence of Lithium Anode Voiding in Argyrodite Solid-State Batteries. *ACS Appl. Mater. Interfaces* **2021**, *13*, 22708-22716.

(58) Li, X.; Liang, J.; Luo, J.; Wang, C.; Li, X.; Sun, Q.; Li, R.; Zhang, L.; Yang, R.; Lu, S.; Huang, H.; Sun, X. High-Performance Li–SeS_x All-Solid-State Lithium Batteries. *Adv. Mater.* **2019**, *31*, 1808100.

(59) Hakari, T.; Hayashi, A.; Tatsumisago, M. Li_2S-Based Solid Solutions as Positive Electrodes with Full Utilization and Superlong Cycle Life in All-Solid-State Li/S Batteries . *Adv. Sustain. Syst.* **2017**, *1*, 1700017.

(60) Santhosha, A. L.; Nazer, N.; Koerver, R.; Randau, S.; Richter, F. H.; Weber, D. A.; Kulisch, J.; Adermann, T.; Janek, J.; Adelhelm, P. Macroscopic Displacement Reaction of Copper Sulfide in Lithium Solid-State Batteries. *Adv. Energy Mater.* **2020**, *10*, 2002394.

(61) Xu, S.; Kwok, C. Y.; Zhou, L.; Zhang, Z.; Kochetkov, I.; Nazar, L. F. A High Capacity All Solid-State Li-Sulfur Battery Enabled by Conversion-Intercalation Hybrid Cathode Architecture. *Adv. Funct. Mater.* **2021**, *31*, 2004239.

(62) Suzuki, K.; Mashimo, N.; Ikeda, Y.; Yokoi, T.; Hirayama, M.; Kanno, R. High Cycle Capability of All-Solid-State Lithium-Sulfur Batteries Using Composite Electrodes by Liquid-Phase and Mechanical Mixing. *ACS Appl. Energy Mater.* **2018**, *1*, 2373–2377.

(63) Hatzell, K.; Zheng, Y. Prospects on Large-Scale Manufacturing of Solid-State Batteries. *MRS Energy Sustain.* **2021**, *8*, 33-39.

(64) Frankel, D. SOLID POWER The Leading Developer of All Solid-State Batteries (ASSB) for Mobile Power Markets https://www1.grc.nasa.gov/wp-content/uploads/12.-SolidPower.pdf (accessed Jul 27, 2021).